Characteristic wave speeds in the surface Brillouin scattering measurement of elastic constants of crystals

A. G. Every,[1,*] L. M. Kotane,[1] and J. D. Comins[1,2]
[1]*Materials Physics Research Institute, School of Physics, University of the Witwatersrand, Johannesburg, Wits 2050, South Africa*
[2]*DST/NRF Centre of Excellence in Strong Materials, University of the Witwatersrand, Johannesburg, Wits 2050, South Africa*
(Received 15 April 2010; revised manuscript received 17 May 2010; published 10 June 2010)

A simple and robust fitting procedure is presented for determining the three elastic constants of a cubic crystal from surface Brillouin scattering measurements carried out in the ⟨100⟩ and ⟨110⟩ directions in a (001) surface. The input data utilized are the Rayleigh surface wave velocity, the Lamb shoulder threshold velocity, and the longitudinal lateral wave velocity measured in the two directions. In fitting these velocities, use of simple closed-form expressions is made for the secular functions determining them. Corresponding expressions for the ⟨010⟩ and $\langle 10\bar{1}\rangle$ directions in the (101) plane are also provided. The formulas for the Lamb shoulder threshold, which have not previously been available in the literature, should prove to be particularly useful, as they apply also to thin supported film structures. The procedure is applied to the determination of the elastic constants of the ternary semiconductor alloy $InAs_{0.91}Sb_{0.09}$, yielding $C_{11}=74.4$ GPa, $C_{12}=40.5$ GPa, and $C_{44}=37.8$ GPa.

DOI: 10.1103/PhysRevB.81.224303 PACS number(s): 78.35.+c, 43.35.+d, 68.35.Gy

I. INTRODUCTION

Extensive use is made of Brillouin scattering of light for the measurement of the elastic constants of crystals.[1–4] It is a noncontact technique that is applicable to small samples, and the measurements can be carried out as a function of temperature and pressure. The frequency shift of the scattered light is equal to that of the phonon created or annihilated in the scattering, and momentum conservation determines the phonon wave vector. Combining these data for a particular scattering geometry yields an acoustic velocity, and from a suitable set of measured velocities the elastic constants can be determined. In the case of transparent media, the scattering is mediated predominantly by the elasto-optic mechanism and takes place within the bulk of the medium. For opaque media, on the other hand, the scattering takes place near the surface of the sample, is mediated predominantly by the surface ripple mechanism, and there is only wave vector conservation parallel to the surface. It is surface Brillouin scattering (SBS) from opaque samples with which this paper is concerned.

A typical SBS spectrum[2–4] for a homogeneous solid consists of a continuous band known as the Lamb shoulder which extends from a lower frequency cutoff or threshold to high frequencies and which arises from scattering by bulk phonons impinging on the surface. Below the cutoff and separated from the Lamb shoulder is commonly to be observed a sharp resonance pertaining to scattering by Rayleigh surface phonons. Often a distinct dip (or a peak if there is some elasto-optic scattering) can be discerned within the Lamb shoulder at what is termed the longitudinal lateral wave (LLW) velocity, which is the threshold for scattering from bulk longitudinal phonons. There are other lateral waves or transonic states as we will refer to them in this paper, that could in principle be detected, but this would require greater sensitivity and signal to noise than is normally achievable with SBS. Not uncommonly, pseudosurface acoustic waves (PSAWs) show up in SBS spectra. These are Rayleigh-type waves that lie within the Lamb shoulder and through coupling to the bulk wave continuum are leaky rather than true unattenuated surface waves.

In determining the elastic constants $C_{\alpha\beta}$ of a crystal from SBS spectra, measurements are usually done in more than one direction in the crystal surface and, if necessary, on two or more differently oriented surfaces; then an optimization fitting procedure is invoked to determine the elastic constants. In this paper we present a particularly simple and robust scheme for recovering the elastic constants of crystals using data pertaining to high-symmetry directions and surfaces for which there is decoupling between sagittally polarized and shear horizontally (SH) polarized motion. The input data for the fitting procedure are the Rayleigh velocity, the Lamb threshold velocity, and the LLW velocity measured in two or more directions. These are fitted using closed-form expressions for the secular functions determining these velocities. The formulas for the Lamb shoulder threshold, which have not previously been available in the literature, should prove to be particularly useful, as they apply also to thin supported film structures. For such structures the Rayleigh velocity is dispersive and the LLW feature evolves with the film thickness to wavelength ratio d/λ (Ref. 5) but the Lamb threshold is an attribute of the substrate and independent of d/λ. As an illustrative example, we apply the procedure to determining the elastic constants C_{11}, C_{12}, and C_{44} of a cubic crystal of the ternary semiconductor alloy $InAs_{0.91}Sb_{0.09}$, using measurements carried out on the ⟨100⟩ and ⟨110⟩ directions in the (001) surface.

II. SURFACE BRILLOUIN SCATTERING THEORY

We consider scattering from an anisotropic solid occupying the half space $x_3>0$. For the 180° backscattering geometry commonly used in SBS, the wave vectors of the incident and scattered laser light $\mathbf{k}_i$ and $\mathbf{k}_s$, respectively, lie in a common sagittal plane, and the incident and scattering angles θ_i

and θ_s are equal, i.e., $\theta_i = \theta_s$. The scattering vector parallel to the surface is in magnitude thus

$$k_{\parallel} = 2k_i \sin\theta_i. \tag{1}$$

The frequency shift that the light undergoes on being scattered is equal to the frequency of the phonon created or annihilated, i.e., $|\omega_s - \omega_i| = \omega$. For the Rayleigh wave peak in the SBS spectrum, the surface phonon phase velocity v is thus given by

$$\omega = k_{\parallel} v. \tag{2}$$

The Lamb shoulder is associated with scattering from bulk acoustic phonons incident from all directions on the surface and which have wave vector component parallel to the surface equal to $\mathbf{k}_{\parallel}$. Since there is essentially no restriction on the normal component of the wave vectors of these phonons, their k's and ω's have no upper limit. The lower limit to the Lamb continuum is conditioned by the slow transverse (ST) wave having group velocity parallel to the surface and projected wave vector $\mathbf{k}_{\parallel}$.

The two important mechanisms for the inelastic scattering of light by acoustic phonons are dynamic rippling of the surface of the solid by the phonons and the modulation of the refractive index by the fluctuating strain field of the phonons. For opaque solids such as $InAs_{0.91}Sb_{0.09}$, into which there is only very limited penetration of the light, surface ripple scattering dominates over elasto-optic scattering. In this situation the scattering cross section for frequency shift ω and surface scattering wave vector $\mathbf{k}_{\parallel}$ is proportional to the thermodynamic power spectrum of the normal displacements of the surface at that frequency and wave vector. At room temperature and above, for which $k_B T \gg \hbar\omega$, k_B being Boltzmann's constant, it follows from the fluctuation dissipation theorem that the SBS efficiency or cross section is given by[2–4]

$$I(\omega) = D\frac{T}{\omega}\mathrm{Im}\{G_{33}(\mathbf{k}_{\parallel},\omega)\}, \tag{3}$$

where D is a constant that depends on the optical properties of the medium, the scattering geometry, and the frequency and polarization of the incident light. $G_{33}(\mathbf{k}_{\parallel},\omega) = G_{33}(\mathbf{s}_{\parallel})/\omega$, where $\mathbf{s}_{\parallel} = (s_1, s_2) = \mathbf{k}_{\parallel}/\omega$ is acoustic slowness parallel to the surface, is the Fourier domain surface elastodynamic Green's function for normal force and displacement response, and is given in general as the sum of contributions from three partial waves which are phase matched in the surface by[4]

$$G_{33}(\mathbf{s}_{\parallel}) = i\sum_{n=1}^{3}\frac{adj(\mathbf{B})_3^{(n)}}{\det|\mathbf{B}|}U_3^{(n)}, \tag{4}$$

where

$$B_l^{(n)} = \sum_{pq} C_{3lpq}U_p^{(n)}s_q^{(n)} \tag{5}$$

is the boundary-condition matrix, and C_{pqrs} is the elastic constant tensor of the material, related in the usual way to the Voigt matrix elastic constants $C_{\alpha\beta}$.

The polarization vector $\mathbf{U}$ and slowness vector $\mathbf{s} = (\mathbf{s}_{\parallel}, s_3)$ are related by the Christoffel equations for the bulk medium[6–8]

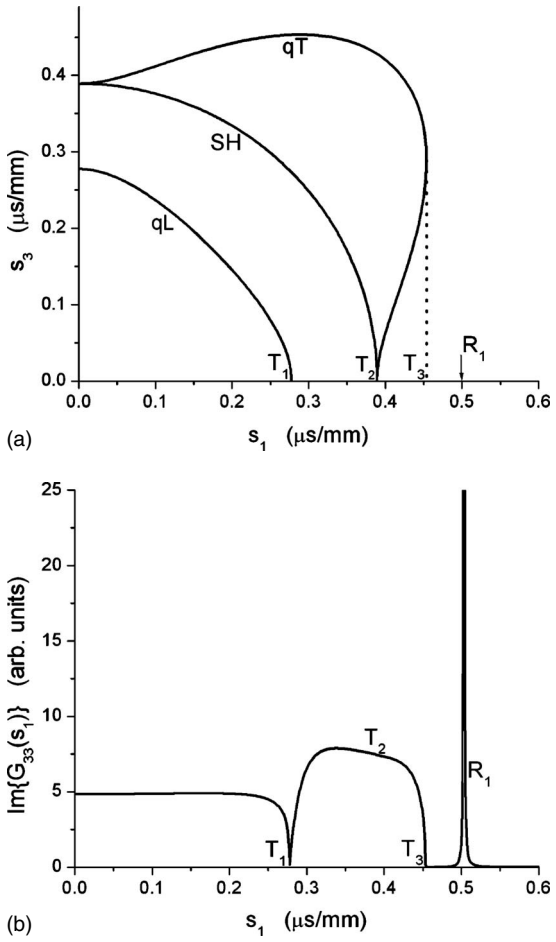

FIG. 1. (a) Positive real solutions of the slowness Eq. (7) for the (010) cube plane of $InAs_{0.91}Sb_{0.09}$. (b) $\mathrm{Im}\{G_{33}(s_1)\}$ for this configuration.

$$(C_{ijkl}s_j s_l - \rho\delta_{ik})U_k = 0 \tag{6}$$

in which ρ is the density. In surface Brillouin scattering $\mathbf{k}_{\parallel}$ and hence $\mathbf{s}_{\parallel}$ is determined by the experimental setup and the scattering geometry, and the slowness component s_3 normal to the surface for each partial wave follows from the characteristic equation of Eq. (6),

$$\det|C_{ijkl}s_j s_l - \rho\delta_{ik}| = 0. \tag{7}$$

This is a sextic equation, which in the case of the surface of the specimen being a materials' symmetry plane becomes a cubic in s_3^2.

A. Transonic states and Rayleigh wave for the ⟨100⟩ direction on the (001) surface

Figure 1(a) shows the (010) cube plane slowness section of $InAs_{0.91}Sb_{0.09}$, i.e., the dependence of the real positive roots s_3 of Eq. (7) on $s_{\parallel} = s_1$ parallel to the ⟨100⟩ cube axis. The calculations have been done using the values of the elastic constants determined later in this paper. This shape of slowness surface is fairly typical of a wide variety of cubic crystals, including the semiconductors Si and Ge, III/V compounds such as GaAs and InSb and metals such as Cu and Fe, for which

$$(C_{12}+C_{44})^2 > C_{11}(C_{11}-C_{44}), \tag{8}$$

which is Appendix A, Eq. (A6) with the replacements $C_{66} \rightarrow C_{44}$ and $C_{22} \rightarrow C_{11}$. The inequality [Eq. (8)] goes hand in hand with the Zener anisotropy factor $\eta = \frac{2C_{44}}{(C_{11}-C_{12})}$ for the medium being appreciably greater than unity. Because the (010) plane is a mirror-symmetry plane, one of the branches, which is labeled SH, pertains to pure T modes SH polarized normal to the (010) plane. As can be inferred from Eq. (A1) of Appendix A by setting C_{55}, $C_{66} \rightarrow C_{44}$ the SH curve is circular, corresponding to constant slowness $s = \sqrt{\rho / C_{44}}$. The other two sheets pertain to quasilongitudinal (qL) and quasitransverse (qT) modes polarized in the sagittal plane. In Fig. 1, T_1, T_2, and T_3 denote extremal values of s_1 or transonic states,[9] where with increasing s_1 two real roots s_3 coalesce and are replaced by pairs of complex-conjugate roots or vice versa. T_3 is the limiting transonic state beyond which all the roots s_3 are complex or pure imaginary. As explained in more detail in Appendix A, it is only when the inequality [Eq. (8)] is satisfied that the qT curve is concave near the s_1 axis and the transonic state T_3 exists. For $InAs_{0.91}Sb_{0.09}$ the left-hand and right-hand sides of Eq. (8) are equal to 6123 GPa^2 and 2723 GPa^2, respectively, so the inequality is well satisfied. For $(C_{12}+C_{44})^2 < C_{11}(C_{11}-C_{44})$ the qT sheet is convex near the s_1 axis, there is no outward bulge, and the limiting transonic state is T_2.

For calculating $G_{33}(\mathbf{s}_\parallel)$ we have written a computer program of a fairly general nature, which can be used for any crystallographic orientation and crystal symmetry. For each $\mathbf{s}_\parallel$ it solves [Eq. (7)] for s_3, and from the six solutions selects the three which in the case of real s_3 correspond to waves with energy flux directed away from the surface and in the case of complex s_3 correspond to inhomogeneous waves whose amplitudes fall off to zero at infinity. As a consequence, the transonic states, where the partial waves change in nature from homogeneous to inhomogeneous, are accompanied by distinctive features in the Green's function. Actually, because for the configuration being considered here the crystal surface and sagittal plane are crystal symmetry planes, the SH polarized mode makes a zero contribution to $G_{33}(\mathbf{s}_\parallel)$ but this is not imposed *a priori* in the program. Figure 1(b) shows $\mathrm{Im}\{G_{33}(s_1)\}$ calculated for the above-mentioned configuration. It is characterized by a sharp intense resonance at the Rayleigh wave slowness R_1 (some damping has been introduced into the calculations to broaden it out from a delta function and render it visible in the figure) and the Lamb shoulder continuum extending from the limiting transonic state T_3 (the Lamb shoulder threshold) down to $s_1=0$. There is a slight kink at the transonic state T_2 (it can be more pronounced for some crystals, depending on the values of the elastic constants) and a sharp minimum at the longitudinal transonic state T_1, also known variously as the LLW, high-frequency pseudosurface mode, longitudinal resonance, and leaky longitudinal surface wave. In crystals for which $(C_{12}+C_{44})^2 < C_{11}(C_{11}-C_{44})$ the Lamb shoulder threshold is the transonic state is T_2.

The velocities of the Rayleigh mode and transonic states are discrete quantifiable attributes of a SBS spectrum that one can anticipate being able to measure with reasonable accuracy, whereas absolute intensities and their continuous variation are much more difficult to establish. Not surprisingly therefore, there have been numerous publications in which the elastic constants of crystals have been determined by fitting to measurements of the Rayleigh and LLW velocities for various scattering configurations. We are only, however, aware of one prior use of measured Lamb shoulder threshold velocities in the determination of the elastic constants of anisotropic solids by Carlotti *et al.*[10] The reason for this has most likely been the nonavailability before now of analytical expressions for this velocity (Carlotti *et al.*[10] in their fitting procedure used the edge of their numerically determined phonon power spectrum). In the present paper we provide expressions for the Lamb threshold and meld them into a systematic and robust optimized fitting procedure in which as many measurable discrete velocities as possible are brought in. Rather than carrying out a least-squares fit to measured velocities, we find it advantageous to use a merit function constructed from secular equations for the discrete velocities cast in a consistent dimensionally equivalent form.

General expressions for the transonic states and Rayleigh mode for the ⟨100⟩ direction in the (010) plane of an orthorhombic crystal are set out in Appendices A and B, respectively, and are adapted in this and the next sections for the cube and diagonal planes in cubic symmetry. Expressions for the ⟨100⟩ direction in the (001) cube plane are obtained by making the replacements C_{55}, $C_{66} \rightarrow C_{44}$, and $C_{22} \rightarrow C_{11}$ in Eqs. (A8) and (A9). Thus the T_1 and T_2 transonic states in Fig. 1 correspond to longitudinal and transverse waves with wave and ray vector (which is normal to the slowness surface) parallel to the ⟨100⟩ direction. Their phase velocities V are determined respectively by the secular equations

$$H_{T1}(\xi, C_{\alpha\beta}) = \xi - C_{11} = 0, \tag{9}$$

$$H_{T2}(\xi, C_{\alpha\beta}) = \xi - C_{44} = 0, \tag{10}$$

where $\xi = \rho V^2$.

The T_3 transonic state corresponds to a qT wave with ray but not wave vector in the ⟨100⟩ direction. Its phase velocity V is determined by the secular Eq. (A7), namely,

$$H_{T3}(\xi, C_{\alpha\beta}) = \xi - E - F\xi^2 = 0. \tag{11}$$

The coefficients E and F, defined in Appendix A simplify in this case to

$$E = \frac{(C_{11}-C_{12})(C_{11}+C_{12}+2C_{44})}{2(C_{11}+C_{44})}, \tag{12}$$

$$F = \frac{(C_{11}-C_{44})^2}{2(C_{11}+C_{44})(C_{11}+C_{12})(C_{11}-C_{12}-2C_{44})}. \tag{13}$$

The Rayleigh wave is in general a superposition of three phase-matched evanescent waves that satisfies the free-surface boundary conditions. Its velocity is governed by the vanishing of the boundary-condition determinant $\det|\mathbf{B}|$. For a general direction of propagation in an arbitrarily oriented surface of an anisotropic solid, calculating this velocity analytically is not a viable option since it is known that the secular equation could be a degree as high as 27 in the vari-

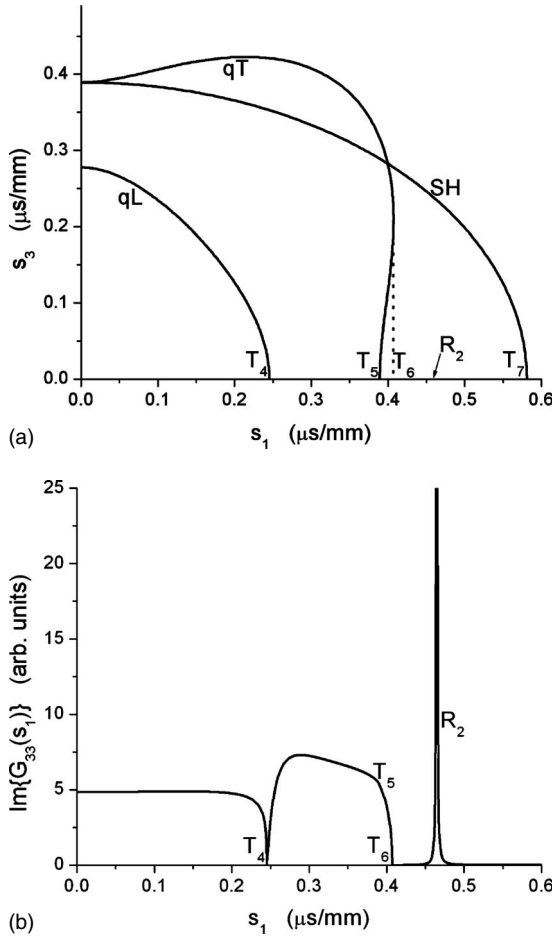

FIG. 2. (a) Positive real solutions of the slowness Eq. (7) for the $(\bar{1}10)$ diagonal plane of $InAs_{0.91}Sb_{0.09}$. (b) $Im\{G_{33}(s_1)\}$ for this configuration.

able ρV^2.[11–13] It is common practice therefore to resort to numerical methods in calculating the Rayleigh velocity. However, in situations where the surface and sagittal planes are materials' symmetry planes there is considerable simplification, in that the shear horizontal mode is decoupled from the other two sagittally polarized modes and the Rayleigh wave is a superposition then just of the latter two. Such two-component Rayleigh or generalized Rayleigh waves (see Appendix B for the distinction) have been studied by a number of authors[14–16] and are governed by relatively simple secular equations. The Rayleigh velocity from Eq. (B1) Appendix B by making the replacements $C_{66} \rightarrow C_{44}$ and $C_{22} \rightarrow C_{11}$ is determined by the secular equation

$$H_{R1}(\xi, C_{\alpha\beta}) = \xi - \left(\frac{C_{11}}{C_{44}} \times \frac{C_{44} - \xi}{C_{11} - \xi}\right)^{1/2} \times (C_{11} - C_{12}^2/C_{11} - \xi) = 0. \tag{14}$$

B. Transonic states and Rayleigh wave for the ⟨110⟩ direction on the (001) surface

Figure 2(a) shows the $(\bar{1}10)$ plane slowness section of $InAs_{0.91}Sb_{0.09}$, i.e., the dependence of the real positive roots s_3 on $s_\parallel = s_1$ parallel to the ⟨110⟩ axis. This is the sagittal plane for propagation in the ⟨110⟩ direction in the (001) plane. Figure 2(b) shows $Im\{G_{33}(s_1)\}$ calculated for this configuration. Again, both crystal surface and sagittal plane are materials' symmetry planes and again there is a sheet of the slowness which is SH polarized and makes a zero contribution in the calculation of $G_{33}(\mathbf{s}_\parallel)$. Secular expressions for the transonic states and Rayleigh wave in the ⟨110⟩ direction in the (001) cube plane are obtained by making the replacements $C_{22} \rightarrow C_{11}$, $C_{66} \rightarrow C_{44}$, $C_{55} \rightarrow (C_{11} - C_{12})/2$, and $C_{11} \rightarrow (C_{11} + C_{12} + 2C_{44})/2$ in Eqs. (A8)–(A10) and (B1). The condition for the qT sheet to be concave near the s_1 axis is

$$(C_{12} + C_{44})^2 > C_{11}(C_{11} + C_{12})/2 \tag{15}$$

and with the left-hand and right-hand sides being equal to 6123 GPa^2 and 4272 GPa^2, respectively, this inequality is also well satisfied for $InAs_{0.91}Sb_{0.09}$. The Lamb shoulder for this situation does not extend to the limiting transonic state T_7 but only to the transonic state T_6. The transonic state T_5 is accompanied by a slight kink in $Im\{G_{33}(s_1)\}$ and the T_4 transonic state, the LLW, by a sharp minimum. Beyond T_6 is the Rayleigh wave. It is supersonic with respect to T_7 but is nevertheless a true nonattenuated SAW because it is uncoupled from the SH polarized ST bulk wave continuum. However, when the direction is tilted away from the symmetry direction it couples to the ST branch, acquires a small ST bulk partial-wave component through which it can be excited and radiate its energy away from the surface, and thereby becomes a leaky or PSAW.

Thus, the T_4 and T_5 and T_7 transonic states in Fig. 2(a) corresponds to longitudinal and transverse waves with wave and ray vector parallel to the ⟨110⟩ direction. Their phase velocities V are determined, respectively, by the secular equations

$$H_{T4}(\xi, C_{\alpha\beta}) = \xi - C = 0, \tag{16}$$

$$H_{T5}(\xi, C_{\alpha\beta}) = \xi - C_{44} = 0, \tag{17}$$

$$H_{T7}(\xi, C_{\alpha\beta}) = \xi - C' = 0 \tag{18}$$

in which

$$C = \frac{1}{2}(C_{11} + C_{12} + 2C_{44}), \tag{19}$$

$$C' = \frac{1}{2}(C_{11} - C_{12}). \tag{20}$$

The T_6 transonic state corresponds to a qT wave with ray but not wave vector in the ⟨110⟩ direction. Its phase velocity V is determined by the secular equation

$$H_{T6}(\xi, C_{\alpha\beta}) = \xi - E - F\xi^2 = 0. \tag{21}$$

The coefficients E and F are as defined in Appendix A with the elastic constant replacements specified in the first paragraph of the present section.

The Rayleigh velocity from Eq. (B1) (Appendix B) by making the above-mentioned replacements is determined by the secular equation

$$H_{R2}(\xi, C_{\alpha\beta}) = \xi - \left(\frac{C_{11}}{C_{44}} \times \frac{C_{44} - \xi}{C - \xi}\right)^{1/2} \left(C - \frac{C_{12}^2}{C_{11}} - \xi\right) = 0. \tag{22}$$

For $InAs_{0.91}Sb_{0.09}$ and other cubic crystal of comparable anisotropy, the Rayleigh wave in the ⟨110⟩ direction described by Eq. (22) is supersonic with respect to the bulk SH wave threshold and exists as a delta function spike in the SH continuum, which however does not feature in $\mathrm{Im}\{G_{33}(s_1)\}$. For directions deviating from ⟨110⟩, the SH continuum now does feature in $\mathrm{Im}\{G_{33}(s_1)\}$ and the limiting transonic state is the Lamb shoulder threshold. The Rayleigh wave now couples to the continuum of bulk SH waves and becomes a PSAW, acquiring a finite resonance width in the process.

In Sec. IV we make use of the simple expressions given above for the SAW and transonic states in the determination of the elastic constants of $InAs_{0.91}Sb_{0.09}$.

C. Transonic states and Rayleigh wave for the (101) surface

For completeness we briefly discuss here the transonic states and Rayleigh waves for the ⟨010⟩ and ⟨10$\bar{1}$⟩ high-symmetry directions in the (101) surface of $InAs_{0.91}Sb_{0.09}$. Figure 3(a) shows the slowness section for $\mathbf{s}_\parallel$ parallel to the ⟨010⟩ axis and Fig. 3(b) shows $\mathrm{Im}\{G_{33}(s_1)\}$ for this configuration while Fig. 4(a) shows the slowness section or $\mathbf{s}_\parallel$ parallel to the ⟨10$\bar{1}$⟩ axis and Fig. 4(b) shows $\mathrm{Im}\{G_{33}(s_1)\}$ for this configuration. In both cases the crystal surface and sagittal plane are materials symmetry planes, and SH polarized branch makes zero contribution to $G_{33}(\mathbf{s}_\parallel)$. Secular expressions for the transonic states and Rayleigh wave in the ⟨010⟩ direction are obtained by making the replacements, $C_{55}, C_{66} \to C_{44}$, $C_{44} \to (C_{11} - C_{12})/2$, and $C_{22} \to (C_{11} + C_{12} + 2C_{44})/2$ in Eqs. (A8)–(A10) and (B1). The condition for the qT sheet to be concave near the s_1 axis is

$$(C_{12} + C_{44})^2 > (C_{11} - C_{44})(C_{11} + C_{12} + 2C_{44})/2, \tag{23}$$

which is well satisfied for $InAs_{0.91}Sb_{0.09}$.

Secular expressions for the transonic states and Rayleigh wave in the ⟨10$\bar{1}$⟩ direction are obtained by making the replacements $C_{11}, C_{22} \to (C_{11} + C_{12} + 2C_{44})/2$, $C_{12} \to (C_{11} + C_{12} - 2C_{44})/2$, $C_{55} \to C_{44}$, and $C_{66} \to (C_{11} - C_{12})/2$ in Eqs. (A8)–(A10) and (B1). The condition for the qT sheet to be concave near the s_1 axis is

$$(C_{11} - C_{44})^2 > (C_{12} + C_{44})(C_{11} + C_{12} + 2C_{44})/2, \tag{24}$$

which for the ⟨10$\bar{1}$⟩ direction is *not* satisfied for $InAs_{0.91}Sb_{0.09}$. The qT sheet is convex near the s_1 direction and the transonic state T_{13}, which determines the Lamb shoulder threshold, is at $s_1 = \sqrt{\frac{2\rho}{(C_{11} - C_{12})}}$. For inequality [Eq. (24)] to be satisfied requires a small or negative value of C_{12} and thereby a value of Zener anisotropy factor appreciably smaller than unity.

III. SURFACE BRILLOUIN SCATTERING MEASUREMENTS ON $InAs_{0.91}Sb_{0.09}$

As an illustrative example we employ the secular equations discussed above to determine the elastic constants of a single cubic crystal of the semiconducting alloy $InAs_{0.91}Sb_{0.09}$.[17–19] This particular ternary alloy has become an important focus in the development of long-wavelength optoelectronic devices due its energy gap corresponding to a wavelength of about 4.2 μm,[20,21] which is within the infrared wavelength range 3–5 μm, the transmission window in the atmosphere. Furthermore, this alloy is reported to have high electron mobility making its application in high-speed devices very attractive.[22] To the best of our knowledge there is no report to date on the measurement of its elastic constants.

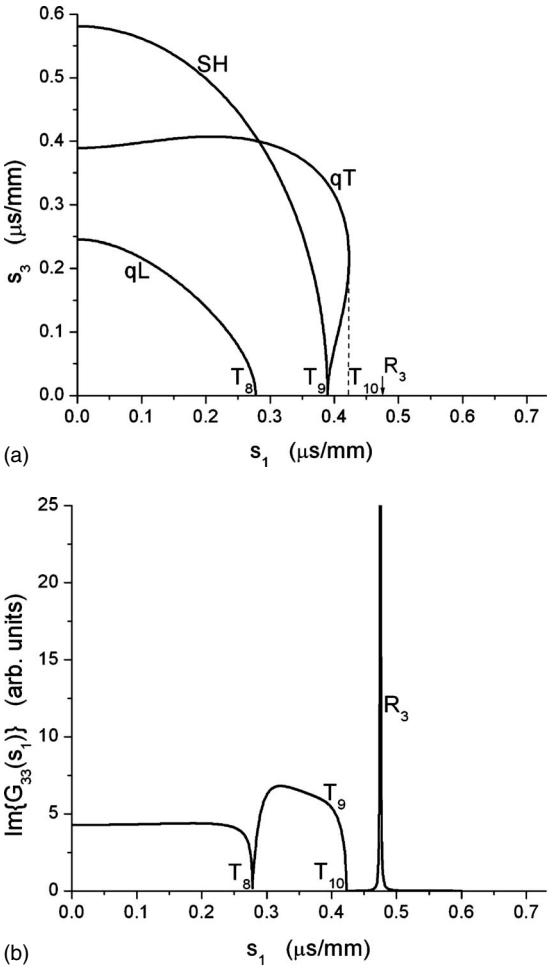

FIG. 3. (a) Positive real solutions of the slowness equation for s_1 in the ⟨010⟩ direction in the (10$\bar{1}$) plane of $InAs_{0.91}Sb_{0.09}$. (b) $\mathrm{Im}\{G_{33}(s_1)\}$ for this configuration, displaying a sharp minimum at T_8 and a slight kink at the transonic state T_9.

We have used SBS to measure the wave speeds of Rayleigh, Lamb threshold, and LLW velocities in the ⟨100⟩ and ⟨110⟩ directions on the (001) surface of $InAs_{0.91}Sb_{0.09}$, which we use in the next section to determine an optimal set of room-temperature values of the elastic constants C_{11}, C_{12}, and C_{44} of the alloy.

$InAs_{0.91}Sb_{0.09}$ specimens with dimensions of about 4 $\times 4$ mm^2 were supplied by J. R. Botha. These undoped samples with a mirrorlike finish were grown by atmospheric pressure metal-organic vapor phase epitaxy on an InAs substrate. Additional information supplied with the ternary alloy

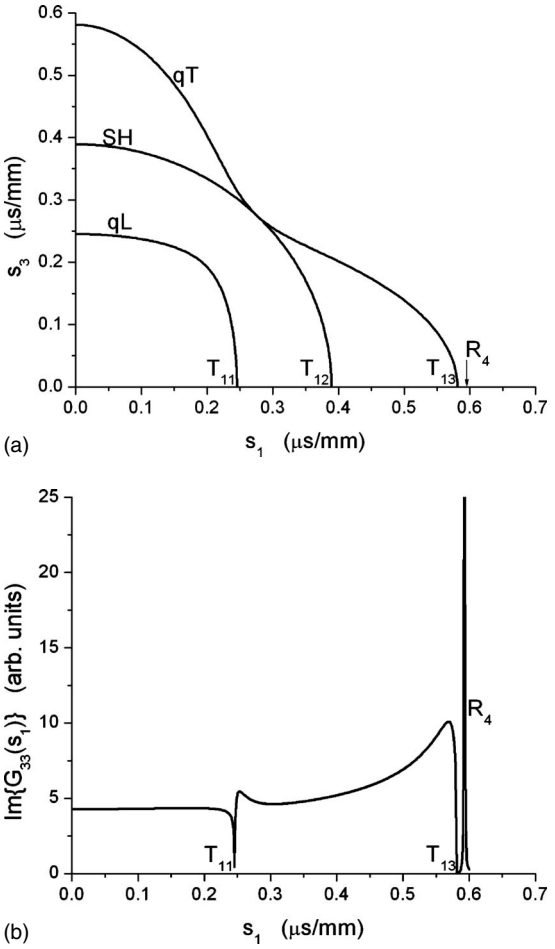

FIG. 4. (a) Positive real solutions of the slowness equation for s_1 in the $\langle 10\bar{1}\rangle$ direction in the (010) plane of $InAs_{0.91}Sb_{0.09}$. (b) $\mathrm{Im}\{G_{33}(s_1)\}$ for this configuration, displaying no trace of the SH transonic state T_{12}.

showed that it was measured to be about 2.7 μm thick by the Nomarski differential interference method, which is thick enough to be regarded as bulk material in SBS and was lattice matched to the (100) orientation of the InAs substrate,.

$InAs_{0.91}Sb_{0.09}$, in common with a number of III-V alloys, forms a crystal with a cubic zinc-blende structure. X-ray diffraction measurements were carried out on the specimen and its room-temperature lattice constant determined to be 6.0811 Å. The density was then calculated from the lattice constant and the total atomic weight in a unit cell to be 5.729 $\mathrm{g/cm^3}$. SBS measurements were commenced after the sample's surface was cleaned with alcohol and acetone to maintain its mirrorlike finish.

The experimental arrangement used for SBS measurements is described in Comins.[3] In brief, measurements were done at room temperature using an argon-ion laser of wavelength 514.5 nm operated in a single axial mode for illumination. The laser light was focused onto the sample by a 120 mm focal length lens and the scattered light was collected with the same lens in the backscattering geometry. The scattered light was analyzed by a Sandercock-type (3+3)-pass tandem Fabry-Pérot interferometer. The light was detected by a silicon avalanche photodiode device. The scattering

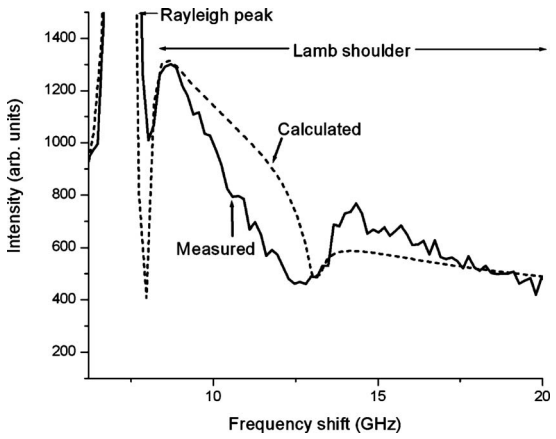

FIG. 5. The measured and calculated SBS spectra for the $\langle 100\rangle$ direction on the (001) surface.

angle $\theta_s=\theta_i=71°$ used in the measurements is close to the maximum cross section for the p-p scattering (polarization in the sagittal plane) cross section.

Figures 5 and 6 show, respectively, the anti-Stokes sidebands of measured SBS spectra pertaining to the $\langle 100\rangle$ and $\langle 110\rangle$ directions in the (001) surface of $InAs_{0.91}Sb_{0.09}$. Superposed on these plots are calculated spectra based on elastic constants C_{11}, C_{12}, and C_{44} to be determined in the next section. Comparison shows a reasonably good agreement between measured and calculated spectra, particularly as regards the Rayleigh modes and the edge of the Lamb shoulder. There is more uncertainty in locating positions of the LLW minima, as is evident when comparing the "valleys" of the measured spectra to the calculated "dips." The transonic states T_2 and T_5 are barely perceptible features even in the calculated spectra and totally obscured by noise in the measured spectra. The discrete features we are therefore able to use in the next section for determining the elastic constants are the Rayleigh velocities R_1 and R_2, the edges of the Lamb shoulders, i.e., transonic states T_3 and T_6 and LLW minima, i.e., transonic states T_1 and T_4.

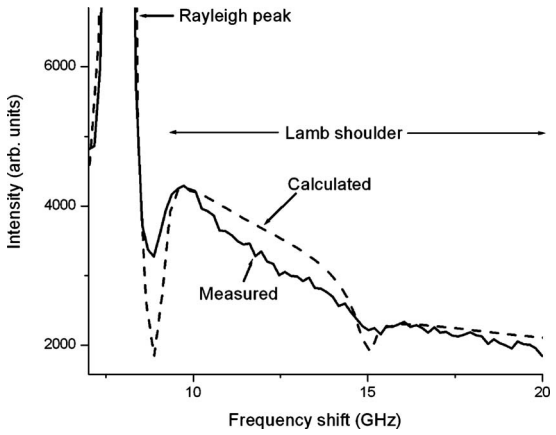

FIG. 6. The measured and calculated SBS spectra for the $\langle 110\rangle$ direction on the (001) surface.

TABLE I. The calculated velocities and their deviations from the measured ones are shown.

Velocity, direction	V_{measured} (m/s)	$V_{\text{calculated}}$ (m/s)	Deviation (%)
V_{R1} ⟨100⟩	2010	1987	−1.14
V_{R2} ⟨110⟩	2138	2152	0.65
V_1 ⟨100⟩	3482	3603	3.48
V_3 ⟨100⟩	2229	2204	−1.12
V_4 ⟨110⟩	4179	4077	−2.44
V_6 ⟨110⟩	2415	2456	1.70

IV. DETERMINATION OF ELASTIC CONSTANTS FROM VELOCITY DATA

In this section we describe the method we have used to calculate the room-temperature values of the elastic constants C_{11}, C_{12}, and C_{44} of $InAs_{0.91}Sb_{0.09}$ from the Rayleigh wave speeds R_1 and R_2 and the transonic states T_1, T_3, T_4, and T_6, measured in the ⟨100⟩ and ⟨110⟩ principal symmetry directions, respectively. With only three parameters to vary, this is an over-determined problem calling for optimal fitting as defined by the minimization of a suitable merit function. The merit function we have adopted for this purpose is

$$\chi^2 = \sum_i w_i H_i^2(\xi_i), \tag{25}$$

summed over $i=T_1,T_3,T_4,T_6,R_1,R_2$, where w_i are relative weightings accorded to the six terms, $H_i(\xi_i;C_{\alpha\beta})\approx 0$ are the secular functions determining the six velocities, cast in the form discussed in Sec. II, and $\xi_i=\rho V_i^2$, where V_i are the six *measured* velocities listed in Table I. They represent velocities for the individual features averaged over the Stokes and anti-Stokes sidebands of the SBS spectra. All six $H_i(\xi_i;C_{\alpha\beta})$ are homogeneous functions of degree 1 in ξ_i and $C_{\alpha\beta}$, and so the derivatives $K_i=\frac{\partial H_i}{\partial \xi_i}$, which come into the weighting factors below, are dimensionless numbers. H_1 and H_4 represent precisely the deviations between the measured and calculated values of ξ_1 and ξ_4, respectively, and so $K_1=K_4=1$ while for the remaining K_i there are additional terms to take into account. From the measured values of the velocities and preliminary estimates of the elastic constants, the terms $F\xi^2$ in Eqs. (11) and (21) are very much smaller than the other terms and so $K_3\approx K_6\approx 1$ while for the Rayleigh wave one finds $K_{R1}\approx K_{R2}\approx 2.5$.

This approach is essentially equivalent to a least-squares fit between measured and calculated velocities V_i^{meas} and V_i^{calc}, respectively, in which the merit function would be taken as

$$\chi^2 = \sum_{i=1}^{6} \frac{(V_i^{meas}-V_i^{calc})^2}{\sigma_i^2} \tag{26}$$

and σ_i are the standard deviations pertaining to the measured data. The use of Eq. (25) is, however, simpler than Eq. (26) in that it obviates the need, in particular, to solve the Rayleigh Eqs. (14) and (22) and Lamb threshold Eqs. (11) and (21), and choose between the resulting roots. A number of investigators have reported elastic constant determination by optimized fitting on the basis of the secular functions for bulk waves in anisotropic solids[23–26] but we are not aware of the secular functions for surface waves and transonic states hitherto being used in this way.

The relative weighting factors in Eq. (25) are related to the standard deviations in Eq. (26) by

$$w_i = A/(V_i\sigma_i K_i)^2, \tag{27}$$

where $A=(V_1\sigma_1K_1)^2$ is a common factor set to render all weightings normalized to $w_{R1}=1$. We have set the values of the remaining w_i as follows. By fitting Lorenzian functions to the prominent SAW and PSAW peaks we find $\sigma_{R1}\approx\sigma_{R2}\approx 44$ m/s. The Lamb shoulder threshold and LLW velocities on the other hand are obtained from less distinct features in the SBS spectrum and we estimate $\sigma_{T1}\approx\sigma_{T3}\approx\sigma_{T4}\approx\sigma_{T6}\approx 2.5\sigma_{R1}$. Using the values of the K_i established above and setting $V_{R1}\approx V_{R2}\approx V_{T3}\approx V_{T6}\approx 2$ mm/μs and $V_{T1}\approx V_{T4}\approx 4$ mm/μs, we are led to the following values for the remaining weightings: $w_{R2}=1$, $w_{T3}=w_{T6}=1$, and $w_{T1}=w_{T4}=0.25$.

With these weighting factors and measured velocities, minimization of χ^2 using Mathematica yields $C_{11}=74.4$ GPa, $C_{12}=40.5$ GPa, and $C_{44}=37.8$ GPa and $\chi^2_{\min}=16.1$ GPa^2. The calculated velocities and their deviations from the measured ones are listed in Table I and are all well within the estimated experimental error in the measured data. We have performed other minimizations keeping $w_{R1}=w_{R2}=w_{T3}=w_{T6}=1$ and varying the value of $w_{T1}=w_{T4}$. A significantly smaller value of $w_{T1}=w_{T4}$ yields poorer fits to V_{T1} and V_{T4} and implausibly accurate fits to V_{R1} and V_{R2} while a significantly larger value of $w_{T1}=w_{T4}$ degrades the fit to V_{R1} and V_{R2} significantly and provides implausibly accurate fits to V_{T1} and V_{T4}. This has convinced us of the reasonableness of the weightings we have used.

Near to the optimum fit, χ^2 can be expressed as a quadratic form in $\delta C_{\alpha\beta}$, the deviations of $C_{\alpha\beta}$ from their optimally fitted values, with the coefficients being proportional to the variances and covariances of the $C_{\alpha\beta}$. An ellipsoid representing the covariance tensor is shown in Fig. 7. There is a factor of about 4.7 between the lengths of the largest and smallest major axes, with the combination of elastic constants $C_{11}-C_{12}+C_{44}$ being the most accurately determined and $C_{11}+C_{12}$ being the least accurately determined.[27]

Within the constraints of thermodynamic stability on the elastic constants, there can be considerable variation in the L, T, and Lamb threshold velocities, these all being dependent on the elastic constants in quite different ways. The Rayleigh velocity on the other hand tends to track the limiting transonic state. For the high-symmetry directions in $InAs_{0.91}Sb_{0.09}$ that we have been considering, the Rayleigh velocity lies between 11% and 14% below the threshold velocity. So, as has been noted before by Carlotti *et al.*,[10] these two velocities for a particular direction are most sensitive to similar combinations of elastic constants. Nevertheless measurements of these two velocities represent statistically independent data and utilizing both in an optimized fitting pro-

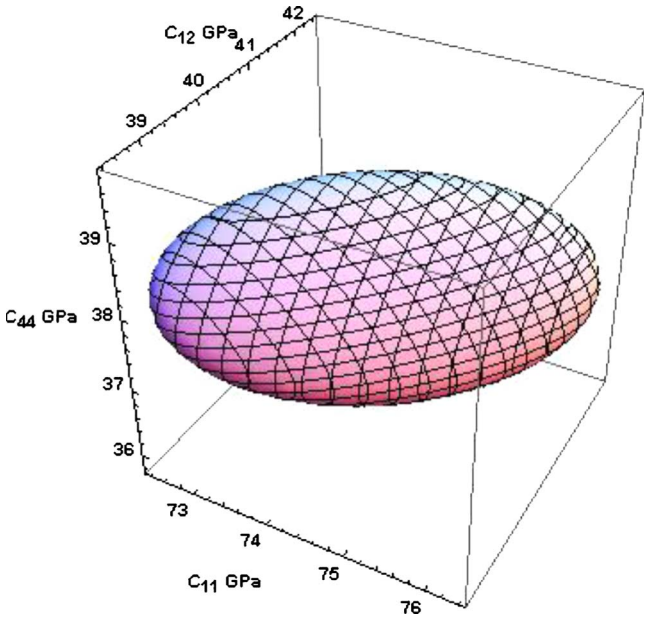

FIG. 7. (Color online) Covariance ellipsoid in elastic constant determination.

cedure must enhance the accuracy of elastic constant determination.

V. CONCLUSIONS

We have shown how SBS measurements of, and secular equations for the Rayleigh, LLW and Lamb shoulder threshold velocities in the ⟨100⟩ and ⟨110⟩ directions in the (001) surface of a cubic crystal can be successfully used in an optimized fitting procedure to determine the three elastic constants C_{11}, C_{12}, and C_{44}. The expressions we have used for the Rayleigh and LLW velocities have previously been available in the literature but the secular equations for the Lamb shoulder are established here. They should prove to be particularly useful, as they apply also to thin supported film structures. The sample we have carried out measurements on and used to demonstrate this procedure is a single crystal of $InAs_{0.91}Sb_{0.09}$. The elastic constants of this crystal, as with many other cubic elements and compounds, comfortably satisfy the inequalities [Eqs. (8) and (15)] for which the Lamb threshold velocities conform to Eqs. (11) and (21). In cases where Eqs. (8) and (15) are clearly not satisfied, then the Lamb threshold velocities are given by the even simpler Eqs. (10) and (18). Usually one will have prior knowledge of approximate values of the elastic constants of a sample, allowing a decision to be made as to which of the formulas to use. In a marginal case where there is doubt, one could do the minimization with different combinations of these formulas and go by the best fit.

ACKNOWLEDGMENTS

This work is based on research supported by the National Research Foundation. J. R. Botha and his research group at the Nelson Mandela Metropolitan University (NMMU) in Port Elizabeth, South Africa are thanked for providing the samples of $InAs_{0.91}Sb_{0.09}$. B. A. Mathe is thanked for help and guidance with the experiments. Helpful advice on the literature has been provided by A. L. Shuvalov.

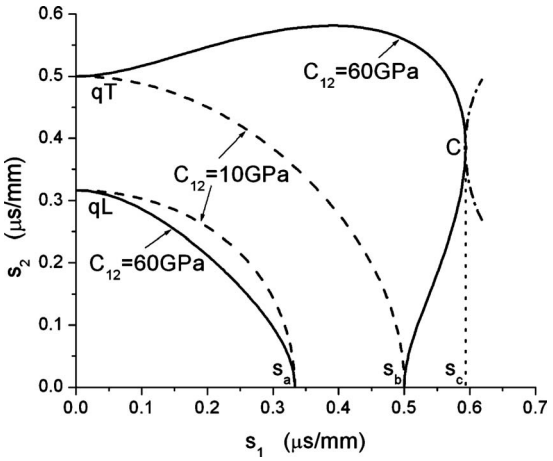

FIG. 8. qL and qT (001) slowness sections for two orthorhombic media with identical $C_{11}=90$ GPa, $C_{22}=100$ GPa, $C_{66}=40$ GPa, and $\rho=10^4$ kg/m^3, but different $C_{12}=10$ GPa (the dashed curves), and $C_{12}=60$ GPa (the solid curves). The dot-dashed curve represents qT branch complex solutions s_2 of the slowness equation. For s_1 near to s_c, $s_2-s_2(s_c)\sim\pm i\sqrt{s_1-s_c}$.

APPENDIX A

We discuss the forms that the (001) symmetry plane section of the acoustic slowness surface of an orthorhombic crystal can take and the implications of these for the transonic states, and the related issue of the Rayleigh wave in the ⟨100⟩ direction in the (010) symmetry plane surface of the half space. The formulas we display are readily adapted to the other symmetry planes of orthorhombic media by index permutations and to the symmetry planes of hexagonal, tetragonal (see Ref. 7 regarding orientation of axes for TII), and cubic media by appropriate interchanges of elastic constants. We assume the common situation in which in all directions the longitudinal wave speed exceeds the transverse wave speed.

Our starting point is the Christoffel secular Eq. (7) which for the (001) symmetry plane section of an orthorhombic medium factorizes into a quadratic equation pertaining to pure transverse modes polarized in the ⟨001⟩ direction[6–8]

$$C_{55}x + C_{44}y - 1 = 0, \tag{A1}$$

where $x=s_1^2/\rho$ and $y=s_2^2/\rho$, and a 2×2 determinantal equation which has the expanded form

$$(C_{11}x + C_{66}y - 1)(C_{66}x + C_{22}y - 1) - (C_{12} + C_{66})^2xy = 0, \tag{A2}$$

pertaining to qT and qL modes polarized in the (001) plane.

Figure 8 depicts qL and qT (001) slowness sections for two orthorhombic media which are identical as regards $C_{11}=90$ GPa, $C_{22}=100$ GPa, $C_{66}=40$ GPa, and $\rho=10^4$ kg/m^3 but have different values $C_{12}=10$ and 60 GPa. The intersec-

tion of the slowness curves along the s_1 axis $s_a=\sqrt{\rho/C_{11}}=0.333$ μs/mm and $s_b=\sqrt{\rho/C_{66}}=0.5$ μs/mm are extremal values of s_1 or transonic states and because of symmetry happen to correspond to pure longitudinal and pure transverse modes, respectively. Not shown is the pure transverse branch which intersects the s_1 axis at $s_d=\sqrt{\rho/C_{55}}$. In the first case, $C_{12}=10$ GPa, represented by dashed curves in Fig. 8, the qT sheet is convex near the ⟨100⟩ direction, and the transonic slowness s_b is a maximum. In the second case, $C_{11}=60$ GPa, represented by solid curves in Fig. 8, the transonic slowness s_b is a minimum and the qT curve is concave near the ⟨100⟩ direction, bulging outward, and then curving backward. There is now a second qT transonic state s_c, lying beyond s_b. This limiting transonic slowness, s_c is conditioned by the vanishing of the derivative $\frac{\partial s_1}{\partial s_2}$, and so is obtained by differentiating [Eq. (A2)] with respect to y and setting $\frac{\partial x}{\partial y}=0$, which yields

$$2C_{22}C_{66}y = x(C_{12}^2 + 2C_{12}C_{66} - C_{11}C_{22}) + (C_{22} + C_{66}). \tag{A3}$$

Substituting Eq. (A3) into Eq. (A2) we obtain the transonic state s_c as the solution of the quadratic equation

$$A + Bx + Dx^2 = 0, \tag{A4}$$

where

$$A = -c_4^2,$$

$$B = c_4c_2 - c_4c_1 - c_5c_6,$$

$$D = c_1c_2 - c_3c_5,$$

$$c_1 = C_{12}^2 + 2C_{12}C_{66} - C_{11}C_{22} + 2C_{66}^2,$$

$$c_2 = C_{12}^2 + 2C_{12}C_{66} + C_{11}C_{22},$$

$$c_3 = C_{12}^2 + 2C_{12}C_{66} - C_{11}C_{22},$$

$$c_4 = (C_{22} - C_{66}),$$

$$c_5 = 2(C_{12} + C_{66})^2,$$

$$c_6 = (C_{22} + C_{66}). \tag{A5}$$

The existence of this second qT transonic state s_c requires that the solutions of Eqs. (A2) and (A3) for both x and y be positive. This is only the case if[6,28]

$$(C_{12} + C_{66})^2 > C_{22}(C_{11} - C_{66}), \tag{A6}$$

the condition being obtained by setting $y \approx 0$ in Eqs. (A2) and (A3) and selecting the solution $x=1/C_{66}$ of Eq. (A2).

The existence of a region of negative curvature near the s_1 axis and positive curvature further out implies a point of inflection in the slowness curve or vanishing Gaussian curvature in the three-dimensional slowness surface, which maps onto a cuspidal edge in the wave surface and caustics in the energy flux radiated by a point or line acoustic source. Such caustics are a prominent feature of the phonon focusing patterns of crystals.[29,30] In the main text above, Eqs. (8), (15), (23), and (24) are adapted from Eq. (A6) for particular directions in cubic crystals. They are precisely the conditions for the emergence of certain caustic structures in the phonon focusing patterns of cubic crystals and correspond, respectively, to Eqs. (12), (17), (13), and (18) of Ref. 30 Overall, the curvature of the slowness surface plays a crucial role in the elastodynamics of anisotropic media.[31]

Equation (A4) is readily rephrased as an equation for the transonic velocity V of rather $\xi=\rho V^2=1/x$, which we cast in the form

$$\xi - E - F\xi^2 = 0, \tag{A7}$$

where $E=-D/B$ and $F=-A/B$, for application in Sec. IV in the fitting of elastic constants to measured threshold velocities. For completeness, the secular equations for the transonic states s_a, s_b, and s_d in terms of ξ are, respectively,

$$\xi - C_{11} = 0, \tag{A8}$$

$$\xi - C_{66} = 0, \tag{A9}$$

$$\xi - C_{55} = 0. \tag{A10}$$

APPENDIX B

There is an extensive literature on closed-form secular equations for the Rayleigh velocity in directions on crystal surfaces where the sagittal plane is a materials' symmetry plane and SH motion is decoupled from sagittal plane motion.[11–16] In this situation the Rayleigh wave is a superposition just of two sagittally polarized inhomogeneous partial waves. A distinction is made between ordinary Rayleigh waves and what are termed generalized Rayleigh waves. For the former, the slowness components normal to the surface of the half space of the two partial waves are pure imaginary and far from the surface the displacement field therefore falls off monotonically in an exponential way. A generalized Rayleigh wave, on the other hand, is characterized by being a superposition of partial waves whose slowness components normal to the surface are complex,[32] having both real and imaginary parts, so that the displacement field oscillates, with an amplitude that falls off exponentially away from the surface. The inequality [Eq. (A6)] represents sufficient condition for the Rayleigh wave to be of the generalized type since the solutions for s_2 of the slowness equation for s_1 lying beyond the limiting transonic state s_c have both a real part [to start with $\approx s_2(s_c)$] and an increasing imaginary part (to start with $\sim i\sqrt{s_1 - s_c}$), as indicated in Fig. 8.

The secular equation for the Rayleigh wave in the ⟨100⟩ direction on the (010) surface of an orthorhombic crystal can be cast in the form[15]

$$\xi - \left(\frac{C_{22}}{C_{66}} \times \frac{C_{66} - \xi}{C_{11} - \xi}\right)^{1/2} \times (C_{11} - C_{12}^2/C_{22} - \xi) = 0, \tag{B1}$$

which applies whether Eq. (A6) is satisfied or not.

*arthur.every@wits.ac.za

[1] M. Grimsditch, in *Handbook of Elastic Properties of Solids, Liquids and Gases*, edited by M. Levy, H. E. Bass, and R. R. Stern (Academic Press, San Diego, 2001), Vol. I, Chap. 14.
[2] P. Mutti, C. E. Bottani, G. Ghislotti, M. Beghi, G. A. D. Briggs, and J. R. Sandercock, in *Advances in Acoustic Microscopy*, edited by A. Briggs (Plenum, New York, 1995), Vol. 1, Chap. 7.
[3] J. D. Comins, in *Handbook of Elastic Properties of Solids, Liquids and Gases*, edited by M. Levy, H. E. Bass, and R. R. Stern (Academic Press, San Diego, 2001), Vol. I, Chap. 15.
[4] M. G. Beghi, A. G. Every, and P. V. Zinin, in *Ultrasonic Nondestructive Evaluation*, edited by T. Kundu (CRC Press, Boca Raton, 2004).
[5] X. Zhang, J. D. Comins, A. G. Every, P. R. Stoddart, W. Pang, and T. E. Derry, Phys. Rev. B **58**, 13677 (1998).
[6] M. J. P. Musgrave, *Crystal Acoustics* (Acoustical Society of America, Sewickley, 2003).
[7] B. A. Auld, *Acoustic Fields and Waves in Solids* (Krieger, Malabar, 1990), Vol. I.
[8] A. G. Every, in *Handbook of Elastic Properties of Solids, Liquids and Gases*, edited by M. Levy, H. E. Bass, and R. R. Stern (Academic Press, San Diego, 2001), Vol. I, Chap. 1.
[9] Transonic states play a key role in existence theorems for SAW, see J. Lothe and V. I. Alshits, Math. Mech. Solids **14**, 16 (2009).
[10] G. Carlotti, D. Fioretto, L. Palmieri, G. Socino, A. Verdini, and C. Rigo, J. Phys.: Condens. Matter **8**, 2265 (1996).
[11] D. B. Taylor, Proc. R. Soc. London A **376**, 265 (1981).
[12] R. M. Taziev, Akust. Zh. **35**, 922 (1989) [Sov. Phys. Acoust. **35**, 535 (1989)].
[13] T. C. T. Ting, Q. J. Mech. Appl. Math. **55**, 297 (2002).
[14] R. Stoneley, Proc. R. Soc. London A **232**, 447 (1955).
[15] D. Royer and E. Dieulesaint, J. Acoust. Soc. Am. **76**, 1438 (1984).
[16] M. Destrade, Mech. Mater. **35**, 931 (2003).
[17] T. Fukui and Y. Horikoshi, Jpn. J. Appl. Phys. **19**, L53 (1980).
[18] G. S. Lee, Y. Lo, F. Lin, S. M. Bedair, and W. D. Laidig, Appl. Phys. Lett. **47**, 1219 (1985).
[19] R. M. Biefeld, J. Cryst. Growth **75**, 255 (1986).
[20] A. Giani, J. Podlecki, F. Pascal-Delannoy, G. Bougnot, L. Gouskov, and C. Catinaud, J. Cryst. Growth **148**, 25 (1995).
[21] S. M. Sze, *Physics of Semiconductor Devices* (Wiley, New York, 1981).
[22] N. V. Zotova, S. S. Kizhaev, S. S. Molchanov, T. B. Popova, and Yu. P. Yakovlev, Semiconductors **34**, 1402 (2000).
[23] B. Castagnède, J. T. Jenkins, W. Sachse, and S. Baste, J. Appl. Phys. **67**, 2753 (1990).
[24] W. Sachse, B. Castagnede, I. Grabec, K. Y. Kim, and R. L. Weaver, Ultrasonics **28**, 97 (1990).
[25] C. Aristégui and S. Baste, J. Acoust. Soc. Am. **101**, 813 (1997).
[26] C. Aristégui and S. Baste, J. Acoust. Soc. Am. **102**, 1503 (1997).
[27] More precisely, the principal axes of the covariance ellipsoid are oriented in (C_{11}, C_{12}, C_{44}) parameter space along the directions $(0.62, -0.49, 0.61)$, $(-0.35, 0.52, 0.78)$, and $(0.70, 0.69, -0.15)$.
[28] Existence criteria for concavities in slowness sections have been established by V. I. Alshits and P. Chadwick, Wave Motion **25**, 347 (1997).
[29] J. P. Wolfe, *Imaging of Phonons* (Cambridge University Press, Cambridge, 1998).
[30] A. G. Every, Phys. Rev. B **24**, 3456 (1981).
[31] For a review, see, e.g., A. G. Every, in *Handbook of Elastic Properties of Solids, Liquids and Gases*, edited by M. Levy, H. E. Bass, and R. R. Stern (Ref. 8), Vol. I, Chap. 4.
[32] A. M. Kosevich, Yu. A. Kosevich, and E. S. Syrkin, Zh. Eksp. Teor. Fiz. **88**, 1089 (1985) [Sov. Phys. JETP **61**, 639 (1985)].